SAND2018-1500J

The Effect of Solvent and Substrate on the Surface Binding Mode of Carboxylate-Functionalized Aromatic Molecules

Janna Domenico[1], Michael E. Foster[2], Erik Spoerke[2], Mark D. Allendorf[2], and Karl Sohlberg[1]

[1]Department of Chemistry, Drexel University, Philadelphia, PA 19104, USA
[2]Sandia National Laboratories, Livermore, CA 94551, USA

Abstract

The efficiency of dye-sensitized solar cells (DSSCs) is strongly influenced by dye molecule orientation and interactions with the substrate. Understanding the factors controlling the surface orientation of sensitizing organic molecules will aid in the improvement of both traditional DSSCs and other devices that integrate molecular linkers at interfaces. Here, we describe a general approach to understand relative dye-substrate orientation and provide analytical expressions predicting orientation. We consider the effects of substrate, solvent, and protonation state on dye molecule orientation. In the absence of solvent, our model predicts that most carboxylic acid-functionalized molecules prefer to lie flat (parallel) on the surface, due to van der Waals interactions, as opposed to the tilted orientation with respect to the surface that is favored by covalent bonding of the carboxylic acid group to the substrate. When solvation effects are considered, however, the molecules are predicted to orient perpendicular to the surface. We extend this approach to help understand and guide the orientation of Metal-Organic Framework (MOF) thin-film growth on various metal-oxide substrates. A two-part analytical model is developed based on the results of DFT calculations and *ab initio* MD simulations that predicts the binding energy of a molecule by chemical and dispersion forces on rutile and anatase TiO_2 surfaces and quantifies the dye solvation energy for two solvents. The model is in good agreement with the DFT calculations and enables rapid prediction of dye molecule and MOF linker binding preference based on the size of the adsorbing molecule, identity of the surface, and the solvent environment.

I. Introduction

Dye-sensitized solar cells (DSSCs) are a promising type of thin-film solar cells because of their low cost, flexibility, and processability[1]. In traditional DSSCs of the type originally reported by Grätzel,[2] light-absorbing dye molecules, typically anchored to the surface by carboxylate groups, inject photo-excited electrons into a semiconductor such as mesoporous titania. The dye is regenerated via an electrolyte (typically $I_3^- \rightarrow I^-$) in contact with a counterelectrode.[3] The first DSSCs used ruthenium dyes, but since then hundreds of dyes of various types have been considered,[4-9] including porphyrins,[8-9] phthalocyanines,[5] push-pull and donor–π–acceptor molecules,[4, 10] and many other n-type organic dyes.[6] Several elegant systematic experimental investigations demonstrate that the orientation and standoff distance of the dye molecule with respect to the surface strongly affect the device efficiency.[5, 11-15] Most of these studies focused on porphyrin dyes, where it has been shown that the functional groups used to bind the dye to TiO_2 and their location and orientation on the dye molecule can be used to systematically vary the tilt angle relative to the surface normal.[12] A quantitative relationship between cell performance and porphyrin tilt angle was demonstrated in the case of Zn-porphyrin, where it was determined that favorable electron recombination times and charge injection rates are associated with the porphyrin bound at small tilt angles.[15] Indirectly, dye molecule orientation has been correlated with aggregation, which decreases the light-harvesting efficiency of the cell.[6, 15] A number of these works employ modifications to dye molecules aimed at controlling orientation and minimizing aggregation. These add complexity to the dye synthesis, however, and can also complicate the sensitization process due to changes in dye solubility. The identity of the solvent used in the sensitizing process is also known to have a strong effect on solar cell efficiency, although the reasons for this are unclear.[12, 15]

An alternative to using synthetic modifications to control both dye orientation and eliminate aggregation is to lock the dye into a crystalline structure. One such approach is to pair DSSCs with metal-organic frameworks (MOFs). MOFs are ordered nanoporous 3D coordination polymers composed of an inorganic part, an ion or cluster, coordinated by organic linkers. MOFs can be utilized in DSSCs in two different ways: 1) as the dye itself or 2) to house dye molecules. In the first case, the MOF linkers, organic building blocks, can be designed to harvest light[16] and in the second case, the nature of the MOF framework can prevent the linkers and dyes from aggregating by isolating traditional dye molecules within their pores; this will effectively impose order throughout the device[17-18]. Whether the device is of the conventional Grätzel type or is sensitized by employing MOFs (MSSC), the orientation in which the sensitizing molecules interact with the substrate will influence the device performance. Moreover, the preferred linker orientation will govern the MOF orientation on the substrate during a step-by-step growth process or atomic layer deposition;[19] this is also of critical importance for the use of MOFs in other electronic device applications, which is an active area of research[20]. These factors have important implications for the band alignment between the dye molecules or MOF and the substrate (e.g. TiO_2), which are critical to the operation of traditional DSSCs.[16]

Dye molecules[21] and MOF linkers[17] are often attached to surfaces by carboxylic acid groups that stabilize the molecule on the surface, improve the efficiency of charge injection from the light-harvesting molecule into the substrate, and for MOFs, establish the film growth direction. These molecules typically also contain a conjugated planar ring system. When bound to a surface by the anchoring -COOH groups, a dye molecule or MOF linker can either be oriented so that the ring system is at an acute angle with respect to the surface normal (more-or-less perpendicular to the surface) or parallel to the surface. A near-perpendicular orientation is driven by chemical binding of the carboxylate group to the surface, while a parallel orientation results when van der Waals (dispersion) forces dominate. Both molecular dynamics (MD) simulations and density functional theory (DFT) have been used extensively to predict the orientation of species on surfaces ranging from alkane thiols[22-24] and silanes[25-26] used to form self-assembled monolayers, to conjugated organic molecules,[27-28] ionic liquids,[29] polymers,[30] rotaxanes,[31] and carbon nanotubes.[29] Surprisingly, only a few studies of dye molecule binding on TiO_2 surfaces have been reported.[32-33] Although these investigations provide considerable fundamental insight, evaluating new systems quickly is difficult, as a large number of computationally-expensive calculations involving systems as large as 10^6 atoms is necessary. Experimental determination of surface orientation is not straightforward either and involves techniques for which considerable data interpretation is required. Consequently, whether a typical sensitization process using a molecular dye is used or an unconventional approach such as a MOF, it is clear that gaining an ability to quickly predict the orientation of molecules bound to the semiconductor surface would be valuable for both design of new sensitizers and optimization of cell performance.

In this report, we describe DFT calculations and *ab initio* MD simulations carried out to quantify the effects of solvent, substrate, and protonation state (pH) on the preferred binding mode of organic molecules on TiO_2. Based on these calculations, we developed an analytical model that predicts dye orientation as a function of molecular structure and solvent and yields insight into the interplay of forces that determine binding orientation.

II. Methods

II.a. Theoretical Approach

We expect that a molecule will bind perpendicularly on a surface if the following condition is true:

$$\Delta E_{\text{perp}} + \Delta E_{\text{solv}} < \Delta E_{\text{par}} + \frac{\Delta E_{\text{solv}}}{2} \quad (1)$$

For ease of understanding, ΔE_{perp} refers to the binding energy associated with the adsorption mode where the molecule is bound covalently and orients roughly perpendicular to the surface, while ΔE_{par} refers to the case where the molecule is adsorbed in a dispersion-dominated parallel orientation. ΔE_{solv} is the solvation energy for a molecule in a specific solvent.

Therefore, the left-hand side of the above inequality is the total energy associated with perpendicular binding and the right side is the total energy associated with parallel binding, because parallel binding exposes only half of the molecule to the solvent.

In our approach, we first computed ΔE_{par} values for twelve polycyclic aromatic hydrocarbons (PAHs) of varying sizes with respect to the rutile 110 and anatase 101 TiO_2 surfaces using density-functional theory. The range of sizes within the training set also allows the size dependence of the dispersion component of the binding energy to be determined. These energies were then fit to a model that predicts the magnitude of the dispersion interaction when the molecule is parallel to the substrate. The energies computed for dispersion-dominated binding were compared to those for perpendicular binding of benzoic acid (ΔE_{perp}), which allows binding to be partitioned into dispersion and chemical components. This partitioning helps determine if there exists a size threshold above which an adsorbate would prefer to bind parallel to the surface when it contains a carboxylic acid group. Solvent effects were considered since fabrication of such devices occurs in solution. The solvation energy (ΔE_{solv}) was estimated for each PAH in acetonitrile and in water to quantify each adsorbate's affinity to each solvent, since an adsorbate's affinity for the solvent used in device fabrication could influence the binding orientation. The presence of solvent also affects the protonation state of the adsorbate.

In our calculations, ΔE_{solv} is computed as a mean with an associated standard deviation. For this reason, in Expression 1 above, both sides of the inequality have a standard deviation. The rearranged inequality, shown in Expression 2 below, therefore has error on only one side of the inequality. For this reason, it can be more convenient to express this condition in terms of Expression 1 or Expression 2 in order to treat both sides of the inequality consistently (Expression 1) or minimize error (Expression 2).

$$\Delta E_{\mathrm{perp}} + \frac{\Delta E_{\mathrm{solv}}}{2} < \Delta E_{\mathrm{par}} \tag{2}$$

Additionally, studies of CO binding to TiO_2 predict that hydroxylate surface influences the binding.[34] Therefore, binding energies of pyridine, benzoic acid, and several PAHs on the hydroxylated anatase 101 surface were computed to compare binding modes on pristine vs. hydroxylated surfaces. Finally, the binding energies of benzoic acid and benzene to TiO_2 were compared with those predicted for two commonly-used MOF substrates, alumina and silica surfaces, to examine the surface dependence of linker binding orientation.

II.b. Computational methods

All electronic structure calculations and *ab initio* Molecular Dynamics (AIMD) simulations were performed using the Vienna Ab initio Simulation Package[35-38] (VASP) within the generalized-gradient approximation using a plane-wave cutoff energy of 400eV. The PW91 exchange-correlation functional[39-40] was used, as it has been successful in modeling similar

systems[41]. Because van der Waals interactions are important here, Grimme's empirical dispersion correction (D2) was incorporated[42]; this method will henceforth be referred to as PW91-D. For the titanium atoms, a pseudopotential was used that treats the semicore p states as valence; for all other atoms, soft pseudopotentials were used[43-44]. The (110) surface of rutile and (101) surface of anatase were chosen for this study because they are the lowest energy surfaces of each of the most common titania polymorphs.[45-46] Each surface was cleaved from the corresponding optimized bulk and consists of three TiO_2 layers. The dimensions of the anatase and rutile surfaces were (21.35 Å x 29.45 Å) and (21.17 Å x 26.56 Å), respectively; the anatase surface consists of 192 titanium atoms and 384 oxygen atoms, and the rutile surface consists of 168 titanium atoms and 336 oxygen atoms. About 30 Å of vacuum space was included in each slab calculation. For computational efficiency, calculations were carried out at only the gamma point in k-space. Geometry optimizations were converged to 0.05eV/Å using the conjugate gradient optimization algorithm. For all surface calculations, the atoms in the bottom TiO_2 layer were frozen to bulk positions while all other atomic positions were optimized.

Binding energies for the dispersion-dominated binding mode, BE_{par}, were computed using the equation below for each molecule on each of the semiconducting substrates.

$$\Delta E_{\mathrm{par}} = E_{\mathrm{surface+adsorbate}} - E_{\mathrm{adsorbate}} - E_{\mathrm{surface}} \quad (3)$$

Binding energies for the covalent binding mode, BE_{perp}, were computed, after consideration of the placement of the acid proton, using an analogous equation:

$$\Delta E_{\mathrm{perp}} = E_{\mathrm{surface+adsorbate}} - E_{\mathrm{adsorbate}} - E_{\mathrm{surface}} \quad (4)$$

For solvent modeling, a number of solvent molecules, consistent with the experimental density, and one adsorbate molecule were arranged in a cubic cell with an edge length of 15Å. For this construction we used Packmol[47] within the Virtual NanoLab suite of builders. AIMD simulations were run at 300K using VASP with the PW91-D functional. All atoms, including hydrogens, were described explicitly. An integration time step of 1 fs was employed and the total length of the run was 10 ps.

To compute the intermolecular interaction energies between various PAHs and solvent molecules, snapshots were taken every 2 ps from which the solvation energy (ΔE_{solv}) was approximated as follows:

$$\Delta E_{\mathrm{solv}} = E_{\mathrm{solvent+adsorbate}} - E_{\mathrm{adsorbate}} - E_{\mathrm{solvent}} \quad (5)$$

where the energies were calculated with single point PW91-D calculations. The 2 ps interval allows for independence among sampling events, since all vibrations with frequencies greater than 17 cm^{-1} will undergo at least one complete oscillation during this period. The solvation energies

reported in the Results section are the averages of the values from those five snapshots, along with their standard deviations.

III. Results

III.a. DFT and AIMD Results

IIIa.1. Dispersion binding

As discussed in the introduction, the molecular orientation is the result of a competition between dispersion and covalent binding to the surface. To determine effect of dispersion in the absence of covalent binding, the adsorption energies of twelve conjugated molecules of increasing size on the anatase 110 and rutile 110 surfaces were computed. The structures of these adsorbates, which are listed in Table 1, are shown in Figure S-1 of the Supplemental Information. This training set was selected because it covers the range of molecular areas typical of dye molecules and MOF linkers and therefore allows for the examination of dispersion binding among molecules without a carboxylic acid group. An adsorbate may explore a large configurational space when it binds to a surface. Typically, these adsorbates bind in such a way that the plane of the molecule is parallel to the plane of the surface (i.e. normal to the surface vector). Additionally, we note the presence of a "nestled" binding mode that is a result of the anatase 101 surface being corrugated instead of perfectly flat; this mode is preferred when more than half of the molecule can nestle, as shown in Figure 1.

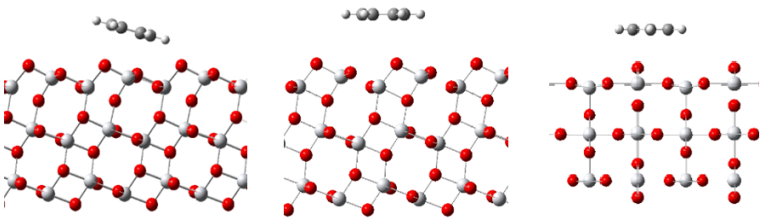

Figure 1. Nestled (left) and non-nestled (center) mode of benzene on the anatase 101 surface; benzene on rutile 110 (right).

The likelihood of nestling depends on the size and area of the adsorbing molecule relative to the corrugation length scale. On anatase 101, if the number of rings that protrude from the surface is less than or equal to the number that can nestle, the adsorbate will nestle. Note that some molecules will only prefer to nestle in the orientations that maximize the number of atoms close to the surface. The largest adsorbates in the training set, ovalene and circumcoronene, are the least likely to nestle, since many more rings will protrude from the surface than will nestle. Consequently, large dyes and MOF building blocks are unlikely to nestle into the surface due to size.

Table 1. Gas phase binding energies of the molecular training set on the rutile 110 and anatase 101 surfaces. N/A indicates that the molecule is too big or otherwise very unlikely to nestle.

	No. aromatic rings	ΔE_{par} (eV)		
		Rutile	Anatase	Anatase Nestled
benzene	1	-2.49	-0.89	-0.99
naphthalene	2	-2.73	-1.23	-1.50
anthracene	3	-3.02	-1.32	-1.79
phenanthrene	3	-2.83	-1.53	-1.83
tetracene	4	-3.78	-1.51	-2.13
pyrene	4	-2.75	-1.43	-1.75
chrysene	4	-3.13	-2.10	-1.81
pentacene	5	-3.30	-2.25	-2.48
benzo[a]pyrene	5	-3.20	-1.78	-1.87
coronene	7	-2.63	-2.29	-2.15
ovalene	10	-3.95	-2.73	N/A
circumcoronene	19	-4.86	-3.30	N/A

III.a.2. Chemical binding

III.a.2.1 Treatment of Acid Proton

Dye molecules and MOF linkers need to be able to anchor to the TiO_2 surface to facilitate charge injection[48]. The preferred binding mode for carboxylic-acid-containing adsorbates on these substrates has been much discussed in the literature[48-62] and there is debate over whether the acid group will be protonated or deprotonated upon adsorption. The incorporation of solvation effects (or lack thereof) and differences between cluster and periodic approaches taken in prior modeling studies make comparing published results difficult[51]. A more comprehensive approach is taken here that considers protonation state and solvation of both the adsorbate and proton. To investigate the binding mode of a carboxylic-acid-containing adsorbate on anatase 101, binding energies were computed for each of several probable orientations of benzoic acid on this surface. This molecule is used as a reference since it is likely that other carboxylated molecules will have a similar adsorption energy to that of benzoic acid when they bind to the surface in a perpendicular orientation, as previously reported.[63] As a simple initial approximation, gas-phase protonated benzoic acid was modeled in perpendicular and parallel orientations onto the anatase surface. These results were compared to two analogous calculations for dissociated benzoic acid where the acid proton is adsorbed onto a nearby surface oxygen. Comparing the binding energies of these four calculations suggests that the protonated benzoic acid binds more strongly than the deprotonated benzoic acid by 0.38 eV. (See Table S-1 of the Supporting Information.)

This prediction is surprising because many experimental results suggest that these adsorbates tend to deprotonate upon adsorption[48, 54, 59, 62]. It is therefore likely that solvation effects

must be included in order to capture the tendency of the adsorbate to deprotonate. To investigate this possibility, in subsequent calculations the acid proton was solvated by a small cluster of 1-3 water molecules. To determine the appropriate number of solvating water molecules, convergence was tested by computing binding energies with the acid proton solvated by one, two, and three water molecules. The results are shown in Figure S-2. Solvation of the acid proton by two water molecules to form the Zündel ion, ($H_5O_2^+$) makes the binding of the deprotonated adsorbate 1.75 eV stronger than the protonated adsorbate, which is in agreement with the literature.[48, 54, 59, 62] We conclude that the theoretically-predicted binding energy value of such an adsorbate is dependent upon the treatment of the proton on the carboxylic acid, and that proton solvation changes benzoic acid's strongest adsorption mode from protonated to deprotonated. Consequently, binding energies of all carboxylic-acid-containing adsorbates in the remainder of this study were computed by considering the adsorbate to be deprotonated with its proton solvated by two water molecules; this is because the structure of the Zündel ion is well-known and energetic convergence with respect to the number of solvating water molecules is nearly reached at two molecules. The energy contribution from proton solvation was computed by taking the average difference between the binding energies of the unsolvated-proton system and dimer-solvated-proton system, which is -2.14 eV (See Table S-1).

III.a.2.2. COO-Ti Binding

For an adsorbate functionalized with a carboxylic acid group on both the rutile 110 and anatase 101 surfaces, we find that the most stable binding mode is bidentate bridging,[50, 61] as shown in Figure 3. As mentioned above, the acid proton is solvated by two water molecules. The binding energies of benzoate on the rutile and anatase surfaces, -5.32 and -3.30 eV, respectively, are much stronger than those produced purely by dispersion in Table 1 due to the formation of Ti-benzoate bonds and the stabilizing effect of the water dimer-proton interaction. Therefore, it is necessary to remove the energetic contribution of the proton solvation (computed above to be -2.14 eV) to determine the energy due only to the Ti-benzoate bonds, yielding ΔE_{perp} values of -3.19 eV for benzoic acid adsorption on rutile and -1.16 eV for anatase. By comparing the ΔE_{par} values for the PAH species listed in Table 1 to those above for benzoate, we predict that carboxylic acid-containing adsorbates on these surfaces will bind perpendicularly via the acid group unless their size is greater than two aromatic rings on anatase 101 and ≥4 aromatic rings on rutile 110. For larger adsorbates, dispersion forces dominate and it becomes energetically favorable to bind in a parallel orientation.

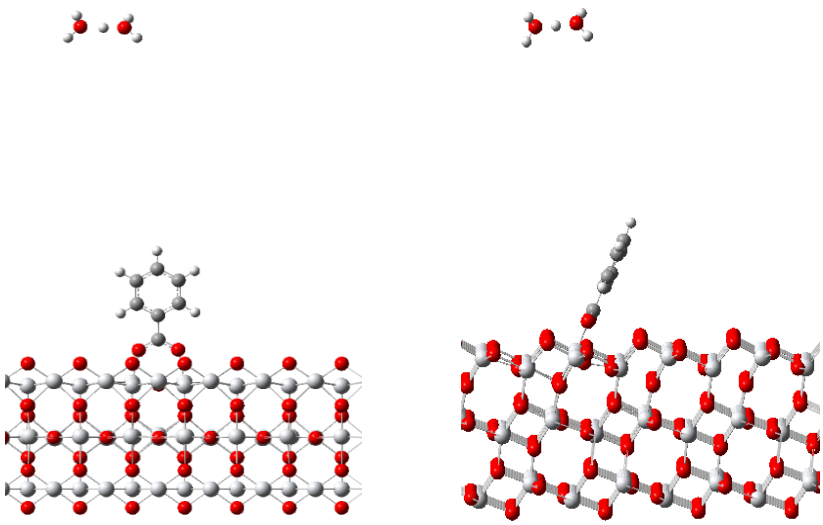

Figure 3. Binding modes for benzoate on the rutile 110 (left) and anatase 101 (right) surfaces with the proton solvated by two water molecules.

III.a.3. Solvation energy

In contrast to the conclusion of the preceding section, there appears to be a general assumption in the literature that even large carboxylic acid-containing dye molecules (≥2 aromatic rings) bind in a nearly-perpendicular orientation on the TiO_2 surface[64]. This discrepancy is likely due to the lack of incorporation of the solvation energy in the calculations reported above (not to be confused with the proton-solvation-energy, which *is* calculated above.) Dye adsorption onto mesoporous anatase for DSSCs and film growth for MOFs occurs in solution, so the gas-phase representation in Figure 3 is not an accurate depiction of the chemical environment during the *staining* or growth process. When an adsorbate binds perpendicularly, the entire molecule is exposed to the solvent, whereas for physisorption, only half of the molecule is solvated. Therefore, if an adsorbate is relatively stable in the solvent - for example, if one considers a polar solvent and an adsorbate with a net dipole moment - a perpendicular binding mode is more likely[65]. This affinity of the molecule for the solvent can be quantified by estimating the solvation energy. The solvation energy for each PAH in acetonitrile and water was estimated as described in the Computational Methods section. The results are listed in Table 2 along with their associated standard deviations; the unsolvated (gas phase) surface binding energies are included for comparison. (See also Table 1.)

Table 2. Estimations of solvation energy for each PAH in acetonitrile and in water. These energies are reported as the average of 5 structures extracted from MD simulations. Gas-phase binding energies for each TiO_2 surface are included for comparison.

	Average Solvation Energy (eV)		Gas phase binding energy ΔE_{par} (eV)	
	Acetonitrile	Water	Rutile	Anatase
benzene	-0.80 ± 0.13	-0.97 ± 0.11	-2.49	-0.99
naphthalene	-1.17 ± 0.09	-1.32 ± 0.16	-2.73	-1.50
anthracene	-1.74 ± 0.15	-2.05 ± 0.15	-3.02	-1.79
phenanthrene	-1.74 ± 0.23	-1.97 ± 0.23	-2.83	-1.83
tetracene	-2.11 ± 0.11	-2.34 ± 0.09	-3.78	-2.13
pyrene	-2.06 ± 0.20	-2.40 ± 0.25	-2.75	-1.75
chrysene	-1.81 ± 0.35	-2.12 ± 0.22	-3.13	-2.10
pentacene	-2.61 ± 0.18	-3.02 ± 0.33	-3.30	-2.48
benzo[a]pyrene	-2.28 ± 0.11	-2.61 ± 0.16	-3.20	-1.87
coronene	-2.53 ± 0.08	-2.84 ± 0.22	-2.63	-2.29
ovalene	-3.28 ± 0.24	-3.63 ± 0.03	-3.95	-2.73
circumcoronene	-4.80 ± 0.21	-5.41 ± 0.28	-4.86	-3.30

The parallel binding energy is considered to be that of the corresponding purely-aromatic molecule from the training set, while the perpendicular binding energy is considered to be equal to that of benzoic acid for all cases. For each adsorbate, there are four possible substrate/solvent combinations.

The specific case of benzene/benzoate is a reasonable model for all systems of one ring. The values for each half of the inequality presented in Expression 1, corresponding to each substrate/solvent combination, are shown in Table 3.

Table 3. Binding Energies for benzoate (perpendicular) and benzene (parallel), computed using expression 2.

	Total Binding Energy (eV)	
	Perpendicular Binding	Parallel Binding
Anatase/Acetonitrile	-1.96 ± 0.13	-1.39 ± 0.07
Anatase/Water	-2.13 ± 0.11	-1.48 ± 0.06
Rutile/Acetonitrile	-3.99 ± 0.13	-2.89 ± 0.07
Rutile/Water	-4.16 ± 0.11	-2.98 ± 0.06

In the absence of uncertainty, perpendicular binding is preferred in each of the four scenarios. Since the solvation energies, and therefore the total energies, do have associated errors, the left- and right-hand sides of the above inequality are each considered a mean (μ) of a

distribution, (assumed normal) with an associated standard deviation, σ. The difference between the distributions is a distribution with an associated mean, μ_{diff}, and standard deviation, σ_{diff}. The values for μ_{diff} and σ_{diff} were used to compute the probability that the binding mode is the opposite from that which the means have predicted. (See Equation S-1 of the Supplemental Information for more detail.) Note that it is more convenient to use the inequality as represented in Expression 1 because both sides incorporate solvent and therefore have associated standard deviations. These probabilities were computed for all 48 adsorbate/solvent/surface combinations; they are shown in Table S-2 in the Supplemental Information. Most confidence values are greater than 80%. For the cases of adsorbates of one aromatic ring in each of the four cases described in Table 3, the means can be trusted with essentially 100% confidence.

III.b. Modeling results

III.b.1. Dispersion binding modeling

We fit the adsorption energies in Table 1 to an analytical model that allows the binding energy of adsorbates on a dry (i.e. solvent-free) TiO_2 surface to be estimated for other molecules. The binding energies of the 12 molecules were fit to a two-term equation of the following form:

$$\Delta E_{\text{par}} = C_1 \frac{n}{r} + C_2 \tag{6}$$

where C_n are constants specific to the TiO_2 polymorph, n is the total number of atoms in the adsorbate, and r is the average distance between an atom in the adsorbate and the plane of the surface. The plane of each surface is considered to be that defined by the outermost layer of atoms excluding the terminating bridging oxygen atoms in each case. Note that anatase binding energies were taken to be the most negative of those of the nestled and non-nestled modes. C_1 and C_2 were first computed for each case by minimizing the sums of squares of the residuals. From this equation, C_2 was kept constant but multiplied by a sigmoidal function such that its contribution goes to zero at large r, which makes the equation more physically realistic and leads to the function,

$$\Delta E_{\text{par}} = C_1 \frac{n}{r} + C_2 \left(\frac{1}{1+e^{(C_3(C_4+r))}} \right), \tag{7}$$

where C_1 and C_2 were kept constant from the first fitting and C_3 and C_4 were computed by again minimizing the sums of squares of the residuals. These values are shown in Table 4 below.

Table 4. Coefficients that minimize the sums of squares of the residuals along with the root mean square error of the predicted values for the parallel-binding-energy model for each substrate.

	Anatase	Rutile
C_1 (eV·Å^6/atom)	-0.127	-0.142
C_2 (eV)	-0.763	-1.915
C_3	8.211	7.635
C_4	-12.457	-8.550

RMSE (eV)	0.156	0.279

III.b.2. Solvation energy modeling

To incorporate solvation effects into the model, the solvation energies of the 12 molecules in each solvent, shown in Table 2, were fit to a two-term equation of the following form:

$$\Delta E_{\text{solv}} = \gamma_1 n + \gamma_2 \quad (8)$$

Where n is the number of atoms of all types in the adsorbate and γ_1 and γ_2 are fitting parameters. Each solvent was fit with a unique set of constants, shown in Table 5, that minimize the sums of squares of the residuals for that data set.

Table 5. Coefficients that minimize the sums of squares of the residuals for the solvation energy expressions.

	Acetonitrile	Water
γ_1 (eV/atom)	-0.0672	-0.0745
γ_2 (eV)	-0.0814	-0.1596
RMSE (eV)	0.1845	0.2048

The model was tested by revisiting the inequality in Expression 2 and substituting the solvation energy and the dispersion binding expressions. It is more convenient here to use the inequality presented in Expression 2 since now each side has an error that is due to the RMSE values presented in Tables 4 and 5; using Expression 1 would introduce more error into each half of the inequality.

$$\Delta E_{\text{perp}} + \frac{\gamma_1 n + \gamma_2}{2} < C_1 \frac{n}{r} + C_2 \left(\frac{1}{1 + e^{(C_3 (C_4 + r))}} \right) \quad (9)$$

The results generated with the model presented in Equation 9 were compared to those generated from the results of the electronic structure calculations. The results of this comparison are summarized in Table S-3 of the Supplemental Information. In all but three cases (chrysene, pentacene, and circumcoronene on anatase in acetonitrile), the model prediction is consistent with the DFT and MD results; for those three cases, the statistical confidence in the DFT and MD result is quite low, rendering the disagreement of little significance. The model offers a way to rapidly compute the probable binding mode of an adsorbate in certain solvent/substrate conditions given the number of atoms in the adsorbate and the average r value from the dataset, which are 3.11 Å and 3.50 Å for anatase and rutile, respectively. The main advantage of the model over the results of the calculations is that the model gives new insight into the factors that favor parallel or perpendicular binding. For acetonitrile/anatase, the point at which the orientational preference changes is predicted to be around 62 atoms; for water/anatase, this point is around 138 atoms. On rutile, this occurs for adsorbates over 192 atoms in size in acetonitrile and 421 atoms in size in water. Although the molecule size and number of atoms is going to be molecule-dependent, ultimately, using water as a solvent instead of acetonitrile will increase the size threshold for

orientational switching to molecules with twice as many atoms; similarly, using rutile instead of anatase will allow this size threshold to increase by three times. These results, shown in Figure 4, show the point of intersection between the parallel and perpendicular binding energy in terms of size of the adsorbate; this point can be engineered by appropriate selection of surface or solvent.

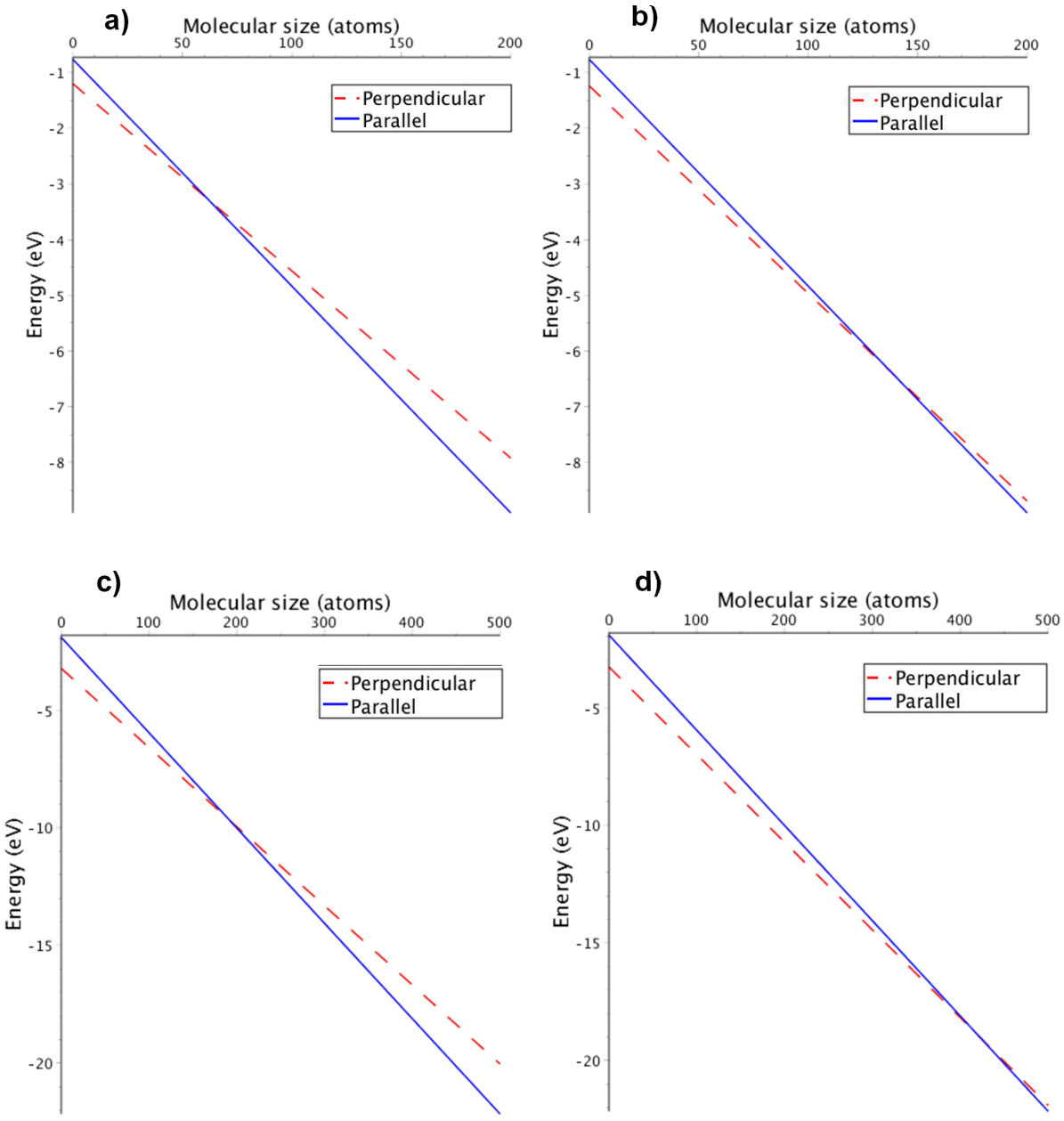

Figure 4. Graphs depicting the competition between solvent and substrate on the preferred binding mode of a dye molecule or linker as a function of size of the adsorbate. **a)** Anatase and Acetonitrile, **b)** Anatase and Water, **c)** Rutile and Acetonitrile, **d)** Rutile and Water

III.c. Saturating the TiO_2 surfaces

III.c.1. The effect of OH groups on anchor binding

Both titanium dioxide surfaces function as Lewis acids[66-68] due to the presence of the five-coordinated Ti atoms at the surface. As a result, exposed unsaturated metal centers are unlikely[69] and it is plausible that the five-coordinated Ti atoms are commonly saturated with OH groups. Therefore, in order for binding to occur, the adsorbate must displace one or more OH groups in order to bind to a surface-exposed Ti atom. Common MOF linkers can have pyridal instead of carboxyl anchors, so for this portion of the study, both benzoic acid and pyridine were considered. To investigate -OH displacement, the binding energies of pyridine and benzoic acid to the OH-terminated anatase 101 surface were computed. Because benzoic acid binds as an anion in a bidentate bridging configuration, but not pyridine. To compare the two, a model was used where the bound adsorbate and three water molecules are generated in each case, with the one or two desorbed OH groups being charge-balanced by hydronium or the Zündel ion. The reaction schemes and optimized structures are depicted in Figs. 4 and 5. The bound benzoic acid case is more stable by 6.41 eV compared to the unbound case, and the bound pyridine case is about 4.00 eV more stable. This supports the use of carboxylic-acid-containing adsorbates as anchors in DSSCs, which reportedly bind more strongly than pyridines due to their preferences for different sites on TiO_2[70] and offer relatively efficient electron injection[65, 71].

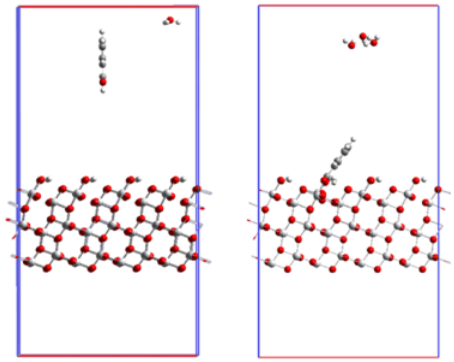

$$C_6H_5COOH + H_3O^+ + (OH^-)_2\text{Surface} \rightarrow C_6H_5COO^- - \text{Surface} + 3H_2$$

Figure 5. Bidentate binding of benzoic acid to the OH-terminated anatase 101 surface. The image at left depicts before binding, while right depicts after.

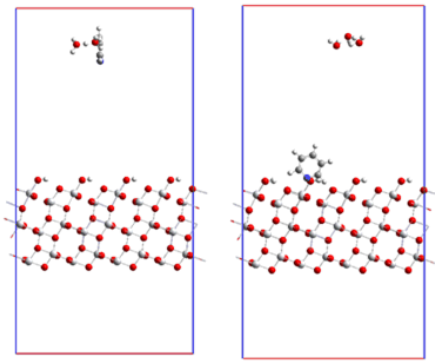

$$NC_5H_5 + H_5O_2^+ + (OH^-)Surface \rightarrow NC_5H_5 - Surface + 3H_2O$$

Figure 6. Binding of pyridine to the OH-terminated anatase 101 surface. The image at left depicts before binding, while right depicts after.

To determine how the presence of OH groups affects the results presented above, the PAH/OH-terminated surface binding energies were computed at the PW91-D level. It was determined, however, that the OH groups drastically inhibit the binding of the purely aromatic adsorbates (parallel binding mode), with the adsorbate removing the OH groups or breaking apart under the influence of these groups. This finding is consistent with the fact that TiO_2 is used in water purification as an agent to break down organic molecules[72].

III.c.2. Substrate effect on linker orientation

It is known that MOF-growth is more favorable on some surfaces than others[73]. To investigate the possible effect of choice of substrate on linker orientation, binding energies for benzene and benzoic acid adsorbed on the 0001 surfaces of quartz SiO_2 and alumina were computed for comparison. The benzoic acid binding energies were computed by taking into account the proton-solvation-energies for water as discussed in the Treatment of Acid Proton section above. Both surfaces were considered to be pristine (i.e. not hydroxylated nor hydrated). The results for the alumina and silica surfaces are presented below in Table 7, along with those of TiO_2 for comparison. The relative strengths of binding may be related to the coordination of the surface metal atoms for each surface.

Table 7. Comparison of dispersion and coordinate-covalent binding for different oxide surfaces.

	Binding Energy (eV)	
	Benzene	Benzoic Acid
Alumina	-1.20	-2.24
Silica	-1.14	-4.10
Rutile	-2.49	-5.32
Anatase	-0.99	-3.30

The binding energies computed for benzene and benzoic acid on alumina suggest that the perpendicular binding mode where the proton is adsorbed onto a nearby surface oxygen is more favorable on alumina than it is for TiO_2 (see Treatment of Acid Proton section), so only unsolvated binding energies are reported. This is indictive of strong proton-surface-oxygen interactions[74]. To consider relative strengths of parallel and perpendicular binding on each surface, one must consider the difference between the parallel and perpendicular binding modes. This is smallest for alumina, which suggests that dispersion binding is more favorable over perpendicular binding for smaller adsorbates on alumina than it is for their interactions with anatase and rutile.

For silica, the difference in energy between the parallel and perpendicular modes of binding is the largest (~3 eV); this suggests that carboxylic acid based adsorbates will more heavily favor perpendicular binding on silica than the other surfaces considered. This preference is predicted to be even more pronounced when solvation energy is considered, since the solvation energy will sum with the native perpendicular binding energy in order to further promote the perpendicular orientation. This result can be rationalized by the observation that the surface silicon atoms are more electron-deficient (according to the computation of the Pauling charge[75]) than the other surface metal atoms considered. See Figure S-3 of the Supplemental Information for the structures of the perpendicular binding orientations on silica and alumina.

IV. Discussion

IV.a. Implications for device construction and MOF growth

Our analysis suggests that the following factors influence an adsorbate's preferred surface orientation in a DSSC or the growth direction in MOF thin-films: the identity of the substrate surface, the solvent that is used during fabrication, and the molecule's protonation state. The discussion below is comprised of three subsections: Substrate, Solvent and Model Implementation. Within the first two sections we will discuss the main role of these components and how they can be used to direct orientation. In addition, the effect of the protonation state, which is coupled to the choice of substrate and solvent, will be discussed within those sections. In the final subsection we discuss the potential implementations of our empirical model and how it can be used to estimate an adsorbate's surface orientation.

IV.a.1. Substrate

The strength of the adsorbate-surface interaction depends on the chemical composition, ability to covalently bond (anchor), surface topology and protonation state. Of the surfaces studied, the rutile polymorph of TiO_2, and quartz SiO_2, yield the highest probability of perpendicular binding for carboxylic acid based adsorbates. Additionally, when the TiO_2 surface is exposed to air or in solution, the lack of unsaturated Ti atoms further sways the adsorbate away from anchoring in a perpendicular fashion. On the other hand, substrates like alumina could possibly benefit from first being hydroxylated, since adsorbate-binding to the bare surface was found to be less favorable than for other substrates. Another important consideration is protonation state of the

adsorbate. In some environments, the proton, from the adsorbate, is favored to bond to a surface oxygen of the substrate over being solvated (e.g. forming a Zündel ion). For titania, the preference for perpendicular binding only occurs when the acid proton is solvated, however, for alumina, the perpendicular binding mode is preferred no matter the treatment of the acid proton. These results demonstrate how one might direct MOF growth direction and dye molecule orientation in DSSCs by choice of substrate.

IV.a.2. Solvent

A solvent that is used during DSSC fabrication and MOF growth needs to have a relatively high affinity for the adsorbate of interest. Since we are mainly interested in a solvent that will dissolve the adsorbate, this affinity can be discussed in terms of the dielectric constant of the solvent and dipole moment of the molecule. It should be noted that both acetonitrile and water tend to be sufficient solvents for MOF growth since, according to our results, they both promote perpendicular binding for small to modest size molecules. Water, with its stronger solvation energies compared to those of acetonitrile, appears to be slightly preferred, perhaps due to the higher number density at room temperature, meaning more water molecules are able to surround the adsorbate than acetonitrile molecules. In addition to solvent/adsorbate affinity (solvation energy), it has been determined that solvent classification is also important for device performance. Aprotic solvents are thought to promote high efficiency of such devices (see Reference 76 and the references therein), especially acetonitrile because of its high dielectric constant and its ability to dissolve both inorganic and organic compounds. Conversely, protic solvents like water have been associated with decreased electron-injection efficiency and durability of devices.[76] Since aprotic solvents have been shown to implicate better device performance, perhaps an aprotic solvent with a higher number density than acetonitrile will better promote perpendicular binding while maintaining high efficiency. As noted above, for some surfaces, a molecule will bind perpendicularly if the acid proton is solvated. To promote proton solvation, a strong base should be added to the solvent during fabrication. These results demonstrate the importance of solvent and protonation state and how orientation is influenced by these factors.

IV.b. Model Implementation

The aim of the empirical model is to be able to predict binding preference by solely considering the number of atoms in the adsorbate and the desired substrate/solvent combination, using the inequality in expression 11. All of the molecules used for parameterization are planar; therefore, the model is best suited for planar, highly conjugated, organic molecules, however, we could plausibly expand the utility to make predictions about molecules that are nonplanar. For planar molecules, n is the total number of atoms in the adsorbate, except those belonging to the carboxylic acid group; this number is considered to be the same for both sides of the inequality. If the molecule has large non-planar aspects, the atom count on the right-hand side of the inequality could be adjusted to avoid counting atoms that cannot interact with the surface owing to geometric considerations. The model might be similarly altered to account for an adsorbate that contains

more than one carboxylic acid group; in that case, the first term in the equality should be multiplied by the number of carboxylic acid groups that can interact with the surface.

For example, this model predicts that a benzene-1,3,5-tricarboxylate (BTC) sensitizer will bind perpendicularly to an anatase or a rutile surface; using a value of 6 for n, on anatase, the model predicts that the perpendicular mode is preferred by 0.40eV in acetonitrile and 0.46eV in water. On rutile, the perpendicular mode is predicted to be favored by 1.28eV in acetonitrile and 1.34eV in water. Experimental results show that the HKUST-1 MOF grows mainly in a (111) orientation relative to each a silica and alumina substrate[77]. The (111) plane of this MOF features the BTC linkers oriented perpendicular to the surface, which is in agreement with the model. Given the relative strengths of the titania, silica, and alumina binding, we believe that the same orientation will result if the HKUST-1 MOF were grown on a titania surface. This demonstrates how the models developed for anatase and rutile can be extrapolated to predict growth on silica and alumina.

V. Conclusion

An empirical analytic model has been developed to screen possible sensitizing and MOF linker molecules based on their preferred binding orientation on different metal-oxide substrates and in different solutions. The model is based on fitting free parameters in physically-motivated terms using the results of first-principles electronic structure calculations and MD simulations. It reveals how a competition between surface binding and solvation energies determines binding orientation, and how these factors vary with molecular size and degree of protonation. Insight into the sensitization and MOF film-growth process can be gained by use of this model. Specifically, it can reveal how the direction and orientation of MOF film growth might be modified by altering the substrate, solvent, and protonation state during fabrication. Primarily, an appropriate solvent/substrate pair may be selected to promote perpendicular or parallel binding for the adsorbate of interest (see Figure 4). It is noted that smaller molecules are more likely to bind in a perpendicular orientation under all solvent/substrate conditions, due to minimal van der Waals interactions. Finally, presented here is a novel approach for controlling the orientation of dye molecules and MOF building blocks on semiconducting surfaces. The data suggest that the solvent and substrate employed in the construction of a DSSC or MSSC can be used to achieve a particular orientation. Our model is straightforward to use and provides a practical tool for screening new sensitizers, predicting aggregation, and identifying appropriate solvents. It can also be used to predict MOF growth direction, which extends its value beyond DSSC to applications such as membranes, sensors, and other electronic devices.

VI. Acknowledgements

This work was supported by the U.S. Department of Energy Office of Energy Efficiency and Renewable Energy SunShot Program under award number DE-EE0000990-1634. Sandia National Laboratories is a multimission laboratory managed and operated by National Technology

and Engineering Solutions of Sandia, LLC, a wholly owned subsidiary of Honeywell International, Inc., for the U.S. Department of Energy's National Nuclear Security Administration under contract DE-NA-0003525.

VII. References

1. Hagfeldt, A.; Boschloo, G.; Sun, L.; Kloo, L.; Pettersson, H., Dye-Sensitized Solar Cells. *Chem. Rev.* **2010**, *110*, 6595-6663.
2. O'Regan, B.; Gratzel, M., A low-cost, high-efficiency solar cell based on dye-sensitized colloidal TiO_2 films. *Nature* **1991**, *353*, 737-740.
3. Planells, M.; Pelleja, L.; Clifford, J. N.; Pastore, M.; De Angelis, F.; Lopez, N.; Marder, S. R.; Palomares, E., Energy levels, charge injection, charge recombination and dye regeneration dynamics for donor-acceptor π-conjugated organic dyes in mesoscopic TiO_2 sensitized solar cells. *Energy & Environmental Science* **2011**, *4*, 1820-1829.
4. Albero, J.; Atienzar, P.; Corma, A.; Garcia, H., Efficiency Records in Mesoscopic Dye-Sensitized Solar Cells. *Chemical Record* **2015**, *15*, 803-828.
5. Cid, J. J., et al., Structure-Function Relationships in Unsymmetrical Zinc Phthalocyanines for Dye-Sensitized Solar Cells. *Chemistry-a European Journal* **2009**, *15*, 5130-5137.
6. Hagfeldt, A.; Boschloo, G.; Sun, L. C.; Kloo, L.; Pettersson, H., Dye-Sensitized Solar Cells. *Chem. Rev.* **2010**, *110*, 6595-6663.
7. Mishra, A.; Fischer, M. K. R.; Bauerle, P., Metal-Free Organic Dyes for Dye-Sensitized Solar Cells: From Structure: Property Relationships to Design Rules. *Angewandte Chemie-International Edition* **2009**, *48*, 2474-2499.
8. Odobel, F.; Blart, E.; Lagree, M.; Villieras, M.; Boujtita, H.; El Murr, N.; Caramori, S.; Bignozzi, C. A., Porphyrin dyes for TiO_2 sensitization. *Journal of Materials Chemistry* **2003**, *13*, 502-510.
9. Urbani, M.; Gratzel, M.; Nazeeruddin, M. K.; Torres, T., Meso-Substituted Porphyrins for Dye-Sensitized Solar Cells. *Chem. Rev.* **2014**, *114*, 12330-12396.
10. Hagberg, D. P.; Edvinsson, T.; Marinado, T.; Boschloo, G.; Hagfeldt, A.; Sun, L. C., A novel organic chromophore for dye-sensitized nanostructured solar cells. *Chemical Communications* **2006**, 2245-2247.
11. Hart, A. S.; Chandra, B. K. C.; Gobeze, H. B.; Sequeira, L. R.; D'Souza, F., Porphyrin-Sensitized Solar Cells: Effect of Carboxyl Anchor Group Orientation on the Cell Performance. *Acs Applied Materials & Interfaces* **2013**, *5*, 5314-5323.
12. Imahori, H., et al., Photoinduced Charge Carrier Dynamics of Zn-Porphyrin-TiO_2 Electrodes: The Key Role of Charge Recombination for Solar Cell Performance. *Journal of Physical Chemistry A* **2011**, *115*, 3679-3690.
13. Rochford, J.; Chu, D.; Hagfeldt, A.; Galoppini, E., Tetrachelate porphyrin chromophores for metal oxide semiconductor sensitization: Effect of the spacer length and anchoring group position. *Journal of the American Chemical Society* **2007**, *129*, 4655-4665.
14. Werner, F.; Gnichwitz, J. F.; Marczak, R.; Palomares, E.; Peukert, W.; Hirsch, A.; Guldi, D. M., Grafting Porphyrins (Face-to-Edge/Orthogonal versus Face-to-Face/Parallel) to ZnO en Route toward Dye-Sensitized Solar Cells. *Journal of Physical Chemistry B* **2010**, *114*, 14671-14678.

15. Ye, S., et al., Role of Adsorption Structures of Zn-Porphyrin on TiO2 in Dye-Sensitized Solar Cells Studied by Sum Frequency Generation Vibrational Spectroscopy and Ultrafast Spectroscopy. *Journal of Physical Chemistry C* **2013**, *117*, 6066-6080.
16. Foster, M. E.; Azoulay, J. D.; Wong, B. M.; Allendorf, M. D., Novel metal-organic framework linkers for light harvesting applications. *Chemical Science* **2014**, *5*, 2081-2090.
17. Stavila, V.; Talin, A. A.; Allendorf, M. D., MOF-based electronic and opto-electronic devices. *Chemical Society Reviews* **2014**, *43*, 5994-6010.
18. Spoerke, E. D.; Small, L. J.; Foster, M. E.; Wheeler, J.; Ullman, A. M.; Stavila, V.; Rodriguez, M.; Allendorf, M. D., MOF-Sensitized Solar Cells Enabled by a Pillared Porphyrin Framework. *The Journal of Physical Chemistry C* **2017**.
19. Rochford, J.; Chu, D.; Hagfeldt, A.; Galoppini, E., Tetrachelate Porphyrin Chromophores for Metal Oxide Semiconductor Sensitization: Effect of the Spacer Length and Anchoring Group Position. *Journal of the American Chemical Society* **2007**, *129*, 4655-4665.
20. Stassen, I.; Burtch, N.; Talin, A.; Falcaro, P.; Allendorf, M.; Ameloot, R., An updated roadmap for the integration of metal-organic frameworks with electronic devices and chemical sensors. *Chemical Society Reviews* **2017**, *46*, 3185-3241.
21. McCree-Grey, J.; Cole, J. M.; Evans, P. J., Preferred Molecular Orientation of Coumarin 343 on TiO_2 Surfaces: Application to Dye-Sensitized Solar Cells. *ACS Applied Materials & Interfaces* **2015**, *7*, 16404-16409.
22. Bhandary, D.; Khan, S.; Singh, J. K., Structure and Dynamics of n-Alkanol Monolayers on a Mica Surface. *Journal of Physical Chemistry C* **2014**, *118*, 6809-6819.
23. Cometto, F. P.; Paredes-Olivera, P.; Macagno, V. A.; Patrito, E. M., Density functional theory study of the adsorption of alkanethiols on Cu(111), Ag(111), and Au(111) in the low and high coverage regimes. *Journal of Physical Chemistry B* **2005**, *109*, 21737-21748.
24. Vemparala, S.; Karki, B. B.; Kalia, R. K.; Nakano, A.; Vashishta, P., Large-scale molecular dynamics simulations of alkanethiol self-assembled monolayers. *Journal of Chemical Physics* **2004**, *121*, 4323-4330.
25. Castillo, J. M.; Klos, M.; Jacobs, K.; Horsch, M.; Hasse, H., Characterization of Alkylsilane Self-Assembled Mono layers by Molecular Simulation. *Langmuir* **2015**, *31*, 2630-2638.
26. Roscioni, O. M.; Muccioli, L.; Mityashin, A.; Cornil, J.; Zannoni, C., Structural Characterization of Alkylsilane and Fluoroalkylsilane Self-Assembled Monolayers on SiO_2 by Molecular Dynamics Simulations. *Journal of Physical Chemistry C* **2016**, *120*, 14652-14662.
27. Della Valle, R. G.; Venuti, E.; Brillante, A.; Girlando, A., Molecular Dynamics Simulations for a Pentacene Monolayer on Amorphous Silica. *Chemphyschem* **2009**, *10*, 1783-1788.
28. Viani, L.; Risko, C.; Toney, M. F.; Breiby, D. W.; Bredas, J. L., Substrate-Induced Variations of Molecular Packing, Dynamics, and Intermolecular Electronic Couplings in Pentacene Monolayers on the Amorphous Silica Dielectric. *Acs Nano* **2014**, *8*, 690-700.
29. Huo, F.; Liu, Z. P., Interfacial layering and orientation ordering of ionic liquid around single-walled carbon nanotube: a molecular dynamics study. *Molecular Simulation* **2015**, *41*, 271-280.
30. Lenhart, J. L.; Fischer, D. A.; Chantawansri, T. L.; Andzelm, J. W., Surface Orientation of Polystyrene Based Polymers: Steric Effects from Pendant Groups on the Phenyl Ring. *Langmuir* **2012**, *28*, 15713-15724.

31. Jang, S. S., et al., Molecular dynamics simulation of amphiphilic bistable [2]Rotaxane Langmuir monolayers at the air/water interface. *Journal of the American Chemical Society* **2005**, *127*, 14804-14816.
32. Gundlach, L.; Szarko, J.; Socaciu-Siebert, L. D.; Neubauer, A.; Ernstorfer, R.; Willig, F., Different orientations of large rigid organic chromophores at the rutile TiO_2 surface controlled by different binding geometries of specific anchor groups. *Physical Review B* **2007**, *75*.
33. Nilsing, M.; Persson, P.; Lunell, S.; Ojamae, L., Dye-sensitization of the TiO_2 rutile (110) surface by perylene dyes: Quantum-chemical periodic B3LYP computations. *Journal of Physical Chemistry C* **2007**, *111*, 12116-12123.
34. Scaranto, J.; Giorgianni, S., A DFT study of CO adsorbed on clean and hydroxylated anatase TiO_2 (001) surfaces. *Molecular Physics* **2009**, *107*, 1997-2003.
35. Kresse, G.; Furthmüller, J., Efficient iterative schemes for ab initio total-energy calculations using a plane-wave basis set. *Physical Review B* **1996**, *54*, 11169-11186.
36. Kresse, G.; Furthmüller, J., Efficiency of ab-initio total energy calculations for metals and semiconductors using a plane-wave basis set. *Computational Materials Science* **1996**, *6*, 15-50.
37. Kresse, G.; Hafner, J., Ab initio molecular dynamics for liquid metals. *Physical Review B* **1993**, *47*, 558-561.
38. Kresse, G.; Hafner, J., Ab initio molecular-dynamics simulation of the liquid-metal-amorphous-semiconductor transition in germanium. *Physical Review B* **1994**, *49*, 14251-14269.
39. Perdew, J. P.; Chevary, J. A.; Vosko, S. H.; Jackson, K. A.; Pederson, M. R.; Singh, D. J.; Fiolhais, C., Atoms, molecules, solids, and surfaces: Applications of the generalized gradient approximation for exchange and correlation. *Physical Review B* **1992**, *46*, 6671-6687.
40. Perdew, J. P.; Chevary, J. A.; Vosko, S. H.; Jackson, K. A.; Pederson, M. R.; Singh, D. J.; Fiolhais, C., Erratum: Atoms, molecules, solids, and surfaces: Applications of the generalized gradient approximation for exchange and correlation. *Physical Review B* **1993**, *48*, 4978-4978.
41. Zasada, F.; Piskorz, W.; Gryboś, J.; Sojka, Z., Periodic DFT+D Molecular Modeling of the Zn-MOF-5(100)/(110)TiO_2 Interface: Electronic Structure, Chemical Bonding, Adhesion, and Strain. *The Journal of Physical Chemistry C* **2014**, *118*, 8971-8981.
42. Grimme, S.; Antony, J.; Ehrlich, S.; Krieg, H., A consistent and accurate ab initio parametrization of density functional dispersion correction (DFT-D) for the 94 elements H-Pu. *The Journal of Chemical Physics* **2010**, *132*, 154104.
43. Kresse, G.; Joubert, D., From ultrasoft pseudopotentials to the projector augmented-wave method. *Physical Review B* **1999**, *59*, 1758-1775.
44. Blöchl, P. E., Projector augmented-wave method. *Physical Review B* **1994**, *50*, 17953-17979.
45. Ramamoorthy, M.; Vanderbilt, D.; King-Smith, R. D., First-principles calculations of the energetics of stoichiometric TiO_2 surfaces. *Physical Review B* **1994**, *49*, 16721-16727.
46. Vittadini, A.; Selloni, A.; Rotzinger, F. P.; Grätzel, M., Structure and Energetics of Water Adsorbed at TiO_2 Anatase 101 and 001 Surfaces. *Physical Review Letters* **1998**, *81*, 2954-2957.
47. Martínez, L.; Andrade, R.; Birgin, E. G.; Martínez, J. M., PACKMOL: A package for building initial configurations for molecular dynamics simulations. *Journal of Computational Chemistry* **2009**, *30*, 2157-2164.
48. Srinivas, K.; Yesudas, K.; Bhanuprakash, K.; Rao, V. J.; Giribabu, L., A Combined Experimental and Computational Investigation of Anthracene Based Sensitizers for DSSC:

Comparison of Cyanoacrylic and Malonic Acid Electron Withdrawing Groups Binding onto the TiO_2 Anatase (101) Surface. *The Journal of Physical Chemistry C* **2009**, *113*, 20117-20126.
49. Agosta, L.; Zollo, G.; Arcangeli, C.; Buonocore, F.; Gala, F.; Celino, M., Water driven adsorption of amino acids on the (101) anatase TiO_2 surface: an ab initio study. *Physical Chemistry Chemical Physics* **2015**, *17*, 1556-1561.
50. Chen, K. J.; Charaf-Eddin, A.; Selvam, B.; Boucher, F.; Laurent, A. D.; Jacquemin, D., Interplay between TiO_2 Surfaces and Organic Photochromes: A DFT Study of Adsorbed Azobenzenes and Diarylethenes. *The Journal of Physical Chemistry C* **2015**, *119*, 3684-3696.
51. Fantacci, S.; Lobello, M. G.; De Angelis, F., Everything you always wanted to Know about Black Dye (but Were Afraid to Ask): A DFT/TDDFT Investigation. *CHIMIA International Journal for Chemistry* **2013**, *67*, 121-128.
52. Grinter, D. C.; Nicotra, M.; Thornton, G., Acetic Acid Adsorption on Anatase TiO_2(101). *The Journal of Physical Chemistry C* **2012**, *116*, 11643-11651.
53. Lamiel-Garcia, O.; Fernandez-Hevia, D.; Caballero, A. C.; Illas, F., Adsorption properties of trifluoroacetic acid on anatase (101) and (001) surfaces: a density functional theory study. *Physical Chemistry Chemical Physics* **2015**, *17*, 23627-23633.
54. Landis, E. C.; Jensen, S. C.; Phillips, K. R.; Friend, C. M., Photostability and Thermal Decomposition of Benzoic Acid on TiO_2. *The Journal of Physical Chemistry C* **2012**, *116*, 21508-21513.
55. Ma, J.-G.; Zhang, C.-R.; Gong, J.-J.; Yang, B.; Zhang, H.-M.; Wang, W.; Wu, Y.-Z.; Chen, Y.-H.; Chen, H.-S., The adsorption of α-cyanoacrylic acid on anatase TiO_2 (101) and (001) surfaces: A density functional theory study. *The Journal of Chemical Physics* **2014**, *141*, 234705.
56. Martsinovich, N.; Jones, D. R.; Troisi, A., Electronic Structure of TiO_2 Surfaces and Effect of Molecular Adsorbates Using Different DFT Implementations. *The Journal of Physical Chemistry C* **2010**, *114*, 22659-22670.
57. Nilsing, M.; Lunell, S.; Persson, P.; Ojamäe, L., Phosphonic acid adsorption at the TiO_2 anatase (101) surface investigated by periodic hybrid HF-DFT computations. *Surface Science* **2005**, *582*, 49-60.
58. Sodeyama, K.; Sumita, M.; O'Rourke, C.; Terranova, U.; Islam, A.; Han, L.; Bowler, D. R.; Tateyama, Y., Protonated Carboxyl Anchor for Stable Adsorption of Ru N749 Dye (Black Dye) on a TiO_2 Anatase (101) Surface. *The Journal of Physical Chemistry Letters* **2012**, *3*, 472-477.
59. Thomas, A. G.; Jackman, M. J.; Wagstaffe, M.; Radtke, H.; Syres, K.; Adell, J.; Lévy, A.; Martsinovich, N., Adsorption Studies of p-Aminobenzoic Acid on the Anatase TiO_2(101) Surface. *Langmuir* **2014**, *30*, 12306-12314.
60. Ünal, H.; Gunceler, D.; Gülseren, O.; Ellialtıoğlu, Ş.; Mete, E., Range-Separated Hybrid Density Functional Study of Organic Dye Sensitizers on Anatase TiO_2 Nanowires. *The Journal of Physical Chemistry C* **2014**, *118*, 24776-24783.
61. Vittadini, A.; Selloni, A.; Rotzinger, F. P.; Grätzel, M., Formic Acid Adsorption on Dry and Hydrated TiO_2 Anatase (101) Surfaces by DFT Calculations. *The Journal of Physical Chemistry B* **2000**, *104*, 1300-1306.
62. Nazeeruddin, M. K.; Humphry-Baker, R.; Liska, P.; Grätzel, M., Investigation of Sensitizer Adsorption and the Influence of Protons on Current and Voltage of a Dye-Sensitized Nanocrystalline TiO_2 Solar Cell. *The Journal of Physical Chemistry B* **2003**, *107*, 8981-8987.

63. Lenz, A.; Karlsson, M.; Ojamäe, L., Quantum-chemical investigations of phenol and larger aromatic molecules at the TiO_2 anatase (101) surface. *Journal of Physics: Conference Series* **2008**, *117*, 012020.
64. Zhang, S.; Yang, X.; Qin, C.; Numata, Y.; Han, L., Interfacial engineering for dye-sensitized solar cells. *Journal of Materials Chemistry A* **2014**, *2*, 5167-5177.
65. Martini, L. A.; Moore, G. F.; Milot, R. L.; Cai, L. Z.; Sheehan, S. W.; Schmuttenmaer, C. A.; Brudvig, G. W.; Crabtree, R. H., Modular Assembly of High-Potential Zinc Porphyrin Photosensitizers Attached to TiO_2 with a Series of Anchoring Groups. *The Journal of Physical Chemistry C* **2013**, *117*, 14526-14533.
66. Panayotov, D. A.; Burrows, S.; Mihaylov, M.; Hadjiivanov, K.; Tissue, B. M.; Morris, J. R., Effect of Methanol on the Lewis Acidity of Rutile TiO_2 Nanoparticles Probed through Vibrational Spectroscopy of Coadsorbed CO. *Langmuir* **2010**, *26*, 8106-8112.
67. Scaranto, J.; Giorgianni, S., A quantum-mechanical study of CO adsorbed on TiO_2: A comparison of the Lewis acidity of the rutile (110) and the anatase (101) surfaces. *J. Mol. Struct.: THEOCHEM* **2008**, *858*, 72-76.
68. Martra, G., Lewis acid and base sites at the surface of microcrystalline TiO_2 anatase: relationships between surface morphology and chemical behaviour. *Appl. Catal., A* **2000**, *200*, 275-285.
69. Lun Pang, C.; Lindsay, R.; Thornton, G., Chemical reactions on rutile TiO_2(110). *Chemical Society Reviews* **2008**, *37*, 2328-2353.
70. Harima, Y.; Fujita, T.; Kano, Y.; Imae, I.; Komaguchi, K.; Ooyama, Y.; Ohshita, J., Lewis-Acid Sites of TiO_2 Surface for Adsorption of Organic Dye Having Pyridyl Group as Anchoring Unit. *The Journal of Physical Chemistry C* **2013**, *117*, 16364-16370.
71. Nilsing, M.; Persson, P.; Ojamäe, L., Anchor group influence on molecule–metal oxide interfaces: Periodic hybrid DFT study of pyridine bound to TiO_2 via carboxylic and phosphonic acid. *Chemical Physics Letters* **2005**, *415*, 375-380.
72. Lee, S.-Y.; Park, S.-J., TiO_2 photocatalyst for water treatment applications. *Journal of Industrial and Engineering Chemistry* **2013**, *19*, 1761-1769.
73. Zacher, D.; Baunemann, A.; Hermes, S.; Fischer, R. A., Deposition of microcrystalline [Cu3(btc)2] and [Zn2(bdc)2(dabco)] at alumina and silica surfaces modified with patterned self assembled organic monolayers: evidence of surface selective and oriented growth. *Journal of Materials Chemistry* **2007**, *17*, 2785-2792.
74. Webber, J.; Zorzi, J. E.; Perottoni, C. A.; Moura e Silva, S.; Cruz, R. C. D., Identification of α-Al_2O_3 surface sites and their role in the adsorption of stearic acid. *Journal of Materials Science* **2016**, *51*, 5170-5184.
75. Sohlberg, K.; Pantelides, S. T.; Pennycook, S. J., Surface Reconstruction and the Difference in Surface Acidity between γ- and η-Alumina. *Journal of the American Chemical Society* **2001**, *123*, 26-29.
76. Sumita, M.; Sodeyama, K.; Han, L.; Tateyama, Y., Water Contamination Effect on Liquid Acetonitrile/TiO_2 Anatase (101) Interface for Durable Dye-Sensitized Solar Cell. *The Journal of Physical Chemistry C* **2011**, *115*, 19849-19855.
77. Stavila, V.; Volponi, J.; Katzenmeyer, A. M.; Dixon, M. C.; Allendorf, M. D., Kinetics and mechanism of metal-organic framework thin film growth: systematic investigation of HKUST-1 deposition on QCM electrodes. *Chemical Science* **2012**, *3*, 1531-1540.